Properties and Structural Characterization of Oxide Starch/Chitosan/Graphene Oxide Biodegradable Nanocomposites

Jun Ma, Changhua Liu, Rui Li, Jia Wang

College of Chemistry and Chemical Engineering, Southwest University, 400715, Chongqing, China

Received 22 December 2010; accepted 16 May 2011
DOI 10.1002/app.34901
Published online 1 September 2011 in Wiley Online Library (wileyonlinelibrary.com).

ABSTRACT: Novel chitosan (CS)/oxidized starch (OST)/graphene oxide (GO) nanocomposites (COST/GO-*n*) films are prepared in a casting and solvent evaporation method. Fourier transform infrared spectroscopy, X-ray diffractions, atomic force microscopy, scanning electron microscopy, transmission electron microscopy, thermal gravimetric analysis, tensile testing, and moisture uptake are used to study the structure and properties of these nanocomposites. To indicate the effect of carboxyl groups of OST, some results of the properties of CS/starch/GO nanocomposite (CST/GO-*n*) were selected for control experimentation. Compared with the control CST/GO-*n* series, COST/GO-*n* films, which have the same component ration showed higher tensile strength (σ_b) and lower elongation at break (ε_b). Additionally, in the COST/GO-*n* series, the σ_b increased with an increase of GO loading. However, higher proportion of GO could result in aggregations of GO nanosheets and deterioration of the film properties. Compared with the COST/GO-0, the values of σ_b and water resistance of the COST/GO-4 containing 2.0 wt % of GO were improved by 57.7 and 20.1%, respectively. © 2011 Wiley Periodicals, Inc. J Appl Polym Sci 123: 2933–2944, 2012

Key words: oxidized starch; graphene oxide; chitosan; polymer composites

INTRODUCTION

Bionanocomposites are a new generation of composite materials that have emerged in the frontiers of materials science, life science, and nanotechnology.[1] Most bionanocomposites from renewable resources, for example, cellulose, starch, and proteins[2] have been considered as excellent raw chemical substances for saving petroleum resources and protecting the environment.[3–5] Starch has been used to produce biodegradable films to partially or entirely replace plastic polymers because of its abundant supply, low-cost, good processability, renewability, and ease of physical and chemical modifications.[6–8] However, wide application of starch film is limited by its water solubility and brittleness.[7,9] Therefore, an effective approach improving the situation above is needed. Blending starch with other biodegradable polymer is a convenient and effective method to overcome these drawbacks. Among various degradable polymer materials, chitosan (CS) has attracted considerable attention for its abundant commercial supply and better mechanical properties.[10,11] Chitsan (CS), α(1-4)-linked 2-amino-2-deoxy-β-D-glucopyranose, is derived from chitin, α(1-4)-linked 2-acetamido-2-deoxy-β-D-glucopyranose.[12] In an acidic environment, the amino groups (—NH_2) can be protonated to —NH_3^+ to readily form electrostatic interactions with anionic groups. As one of the most abundant natural polysaccharides, CS is well known for its good biocompatibility, biodegradability, antibacterial properties, and multiple functional groups, CS has been widely investigated for several decades in applications such as biosensors, tissue engineering, separation membranes, food packaging films, artificial skin, and water engineering.[13,14] In fact, starch (ST)/CS blend films have been investigated as potential composites in several studies.[15–18] However, because starch is only partially compatible with CS, the tensile strength and elongation at break of the ST/CS composites were not significantly improved. Thus, the physical properties of ST/CS composites need further improvement to meet the demands of extensive applications.

In this work, a chemically modified starch was obtained when the native pea starch was oxidized by potassium permanganate. Following the oxidation, the glycosyl residues are substituted and the carboxyl groups were introduced. It is hypothesized that the newly introduced carboxyl groups in starch after oxidation will improve compatibility between oxidized starch (OST) and CS molecules. Moreover, nanocomposite technology using nano-fillers such as carbon nanotubes, clay and silica has already proved to be another effective way to improve the mechanical,

Correspondence to: C. Liu (chliu@swu.edu.cn).

electrical and thermal properties of polymers.[19–22] Recently, a new application of graphene oxide (GO) as a nano-filler in polymer matrices to prepare polymer nanocomposites has also been explored and reported.[23–25] GO, an oxygen-rich carbonaceous layered material, is produced by the controlled oxidation of graphite.[26] Each layer of GO is an oxidized graphene sheet commonly referred to as GO.[27] According to recent studies,[28–33] GO consists of covalently attached oxygen groups such as hydroxyl, epoxy, carbonyl, and carboxyl groups.[34,35] Hence, GO is hydrophilic dispersed in water.[36,37] The facts show that GO has so much oxygen-containing functional groups and can disperse well in water, which are able to interact by hydrogen bonding with $-NH_2$ groups of CS and $-COOH$ groups of OST in the aqueous system. GO represents a physical cross-linking agent to obtain interacting polymers, which can promote the miscibility between OST and CS molecules, and then produce a compatible blend with enhanced properties.

In the work, GO as a physical cross-linking agent was used to fabricate OST/CS/GO and ST/CS/GO nanocomposites. The effects of GO loading on the structure and properties of the OST/CS/GO and ST/CS/GO nanocomposites were comparatively investigated.

EXPERIMENTAL PROCEDURE

Materials

The raw material used in this study, field pea starch composed of 35% amylose and 65% amylopectin, was supplied by Nutri-Pea Limited Canada (Portage la Prairie, Manitoba, Canada). CS was purchased at Nantong Xincheng Biological Industrial Limited Company (Nantong, China) with a weight-average molecular weight (M_w) of more than 300,000 g mol^{-1} and >90% degree of deacetylation (DA). Glycerol (99%) and acetic acid (36%) were obtained from Maoye Chemical (Chongqing, China). Graphite powder was purchased from Shanghai Huayi Group Huayuan Chemical Limited Company (Shanghai, China). Hydrogen peroxide (H_2O_2, 30%) was supplied by Chengdu Kelong Chemical Reagent Company (Chengdu, China). Hydrochloric acid, sodium nitrate, potassium permanganate (analytical grade), and sulfuric acid (95–98%) were purchased from Chongqing chuandong Chemical Reagent Factory (Chongqing, China). The water used was distilled and deionized.

OST preparation and determination of degree of oxidation

The OST was prepared by the following method[38]: First, 40 wt % (w/w) starch slurry (total weight of 175 g) was stirred in a water bath. When the temperature reached 50°C, 2.5 mL 3*M* H_2SO_4 and 12.5 mL 2% $KMnO_4$ were added into the starch slurry, respectively. After that, this mixture was stirred at the same temperature until the color changed into milk white (about 2 h). The OST was filtered and washed about 10 times with distilled water, and then air-dried at (40 ± 2)°C for 48 h. The OST was finally obtained and its carboxyl content (determination of degree of oxidation) was determined according to the procedure of Chattopadhyay et al.[39] The value of the carboxyl content was calculated to be 0.0945.

Preparation of GO

GO was prepared from graphite powder by the modified Hummers method.[26] Briefly, 4 g graphite, 2 g $NaNO_3$, and 92 mL H_2SO_4 were mixed in an ice-bath. Subsequently, 12 g $KMnO_4$ was added slowly into the beaker under stirring, and the rate of addition was controlled carefully to prevent the temperature of the suspension from exceeding 20°C. The ice-bath was then removed and the temperature of the suspension brought to 35 ± 5°C, where it was maintained for 30 min. Then, 184 mL water was added slowly into the mixture and it was stirred it for another 30 min. After that, the reaction was terminated by addition of 340 mL of aqueous solution of H_2O_2 (0.05 wt %), resulting in a yellow brown mixture. Finally, the mixture was centrifuged and washed four times with a solution of 10% HCl and five times with water, respectively. GO powder was obtained under vacuum for 48 h at 40°C.

Preparation of the COST/GO-*n* and CST/GO-*n* films

The glycerol-plasticized COST/GO-*n* films were fabricated by the casting and solvent evaporation method. The CS/OST solution was prepared by dissolving 2 g OST and 0.5 g CS in 30 wt % (of OST) glycerol and a 2% (vv^{-1}) aq HAc, respectively, then the two solution was mixed. After that, the suspension was stirred at 95°C for 30 min until the solution became transparent and the CS/OST paste was obtained. Meanwhile, GO was dissolved in 10 mL of water and treated with ultrasound for 45 min to make a homogeneous brown dispersion (1 mg mL^{-1}). Then GO solution (varied from 0 to 3.0 wt % of CS/OST) was added into the CS/OST paste and the mixture was stirred for another 30 min at 65°C, which were coded as COST/GO-*n*, where *n* is run number varied with the percent of GO based on CS/OST. After degassing under vacuum, the composite was poured into a plexiglass plate placed on a level flat surface and dried at 45°C in an oven for

TABLE I
Codes and Crystallinity for COST/GO-*n* and CST/GO-*n* Nanocomposite Films

Series #1[a]					Series #2[a]	
Codes	Crystallinity (%)	OST or ST (g)	CS (g)	GO (g)	Codes	Crystallinity (%)
OST	19.64	2.0	0	0	ST	22.30
COST/GO-0	18.39	2.0	0.5	0	CST/GO-0	19.76
COST/GO-1	16.18	2.0	0.5	0.01	CST/GO-1	18.12
COST/GO-2	15.62	2.0	0.5	0.02	CST/GO-2	16.13
COST/GO-3	14.36	2.0	0.5	0.03	CST/GO-3	14.41
COST/GO-4	10.78	2.0	0.5	0.04	CST/GO-4	12.08
COST/GO-5	13.05	2.0	0.5	0.05	CST/GO-5	13.44
COST/GO-6	15.17	2.0	0.5	0.06	CST/GO-6	16.69

[a] Series #1 corresponds to COST-based series; and series #2 corresponds to CST-based series.

12 h, and the fully dried films were peeled from the glass plate. To serve as experimental controls, the neat starch film, OST film and CS/ST/GO blend films were obtained through the same fabrication process, which were code as ST, OST, and CST/GO-*n*, where *n* is run number, and varied with the percent of GO based on CS/ST. The codes for all films were listed in Table I. Before various characterizations, the resulting films were kept in a conditioning desiccator of 43% relative humidity (RH) for more than 1 week at room temperature to ensure the equilibrium of the water in the films.

APPARATUS

Fourier transform infrared spectroscopy

Fourier Transform Infrared (FTIR) spectra of the nanocomposites were recorded with a Nicolet (Madison, WI) 170SX Fourier transform infrared spectrometer in the wavelength range of 4000–600 cm^{-1}, in the attenuated total reflection mode.

X-ray diffractometry

X-ray diffractometry was performed on a X-ray diffractions (XRD)-3D, PuXi, (Beijing, China) X-ray diffractometer under the following conditions: Nickel filtered Cu Kα radiation ($\lambda = 0.15406$ nm) at a current of 20 mA and a voltage of 36 kV. The scanning rate was 4°/min in the angular range of 3–40°and 5–40° (2θ). The degree of crystallinity of the nanocomposites were calculated by $Xc = \left(\frac{\sum_i A_{ci}}{\sum_i A_{ci} + \sum_i A_{aj}}\right) \times 100\%$, where A_c is the area of the X-ray diffraction curve due to scattering from the crystalline phase, and A_a is the area of the X-ray diffraction curve due to scattering from amorphous.

Transmission electron microscopy (TEM)

TEM micrographs were obtained with a transmission electron microscope (JEM-100CXII, Japan) at an accelerating voltage of 80 kV. Ultrathin sections of selected films were microtomed at room temperature.

Scanning electron microscopy (SEM)

Scanning electron microscope (S-3300 or S3700, HITACHI, Japan) was used to observe the morphologies of cross-sections and surface of the films at an accelerating voltage of 15 kV respectively. The morphologies of the starch and OST were observed at an accelerating voltage of 0.5 kV (S-4800, HITACHI, Japan).

Atomic force microscopy (AFM)

The surface morphologies and roughness of the prepared composites were observed by atomic force microscopy (AFM) (Veeco Instruments, NY) in the tapping mode. The films surfaces were imaged in a scan size of 1×1 μm^2.

Thermal analysis

Thermal gravimetric analysis (TGA) data of the blend films were collected using a TA Instrument model 2010 (TA Instruments, New Castle, PA). The thermo grams were acquired between 25 and 500°C at a heating rate of 10°C/min. Nitrogen was used as the purge gas at a flow rate of 20 mL/min. An empty pan was used as a reference.

Mechanical properties

The tensile strength and elongation at break of the blend films were tested using a Microelectronics Universal Testing Instrument Model Sans 6500 (Shenzhen Sans Test Machine, Shenzhen, China) according to the Chinese standard method (GB 13022-91). All the films were cut into 10 mm wide and 100 mm long strips and mounted between cardboard grips (150 × 300 mm) using adhesive so that the final area exposed was 10 × 50 mm. The

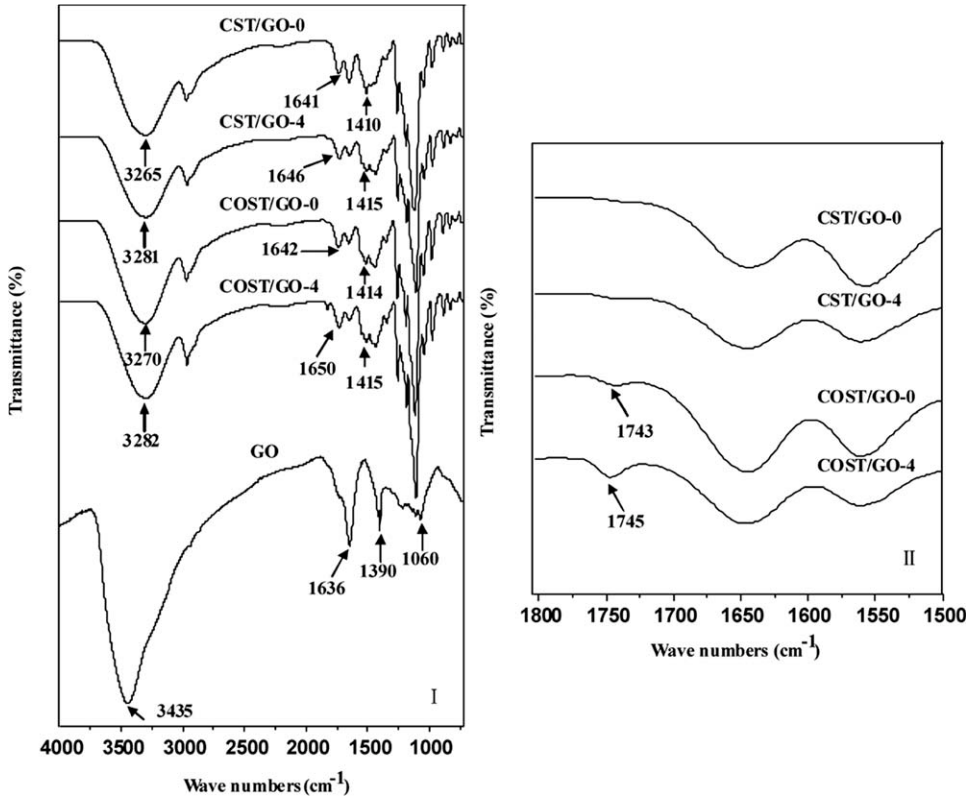

Figure 1 FT-IR spectra of GO, CST/GO-0, CST/GO-3, COST/GO-0, and COST/GO-3 nanocomposites.

crosshead speed was 10 mm/min. All film measurements were performed for five specimens and averaged.

Moisture uptake test

The moisture uptake of the nanocomposite films was determined. The samples used were thin rectangular strips with dimensions of 50 ×10 × 0.1 mm^3. They were dried overnight at 80°C. After the samples were weighed, they were conditioned at 92% RH ($CuSO_4$ saturated solution) for 2 weeks to ensure equilibrium of the moisture before testing. The moisture uptake (M_u) of the samples was calculated as follows:

$$M_u = (W_1 - W_0)/W_0 \times 100\% \quad (1)$$

where W_0 and W_1 were the weight of the sample before exposure to 92% RH and after equilibrium, respectively. An average value of five replicates for each sample was taken.

RESULTS AND DISCUSSION

Structural analysis

To reveal the interactions between GO nanosheets and OST/CS matrix, FTIR spectra of the selected films are shown in Figure 1(a). Additionally, the FTIR spectrum of GO is also tested. The FTIR spectrum of the GO show a broad absorption band at 3435 cm^{-1}, which is related to the OH groups, and absorption bands at 1636 and 1390 cm^{-1}, which are typical of carbonyl and carboxyl groups.[40] For the starch/CS film (CST/GO-0), the broad band at 3265 cm^{-1} was the OH stretching vibrations. The peaks near 2930 cm^{-1} were typical C—H stretching vibrations, whereas the bands at 1641 cm^{-1} and 1410 cm^{-1} were assigned to the δ (O—H) bending of water and CH_2, respectively.[6] The band at 997 cm^{-1} was attributed to the stretching vibration of C—O in the C—O—C groups. For COST/GO-0, the above-mentioned peaks at 3265 and 1410 cm^{-1} in CST/GO-0 shifted to 3270 and 1414, respectively. Those changes were related to the hydrogen bonding in the blends, indicating the oxidation treatment significantly changed the intermolecular and intramolecular hydrogen bonding of starch and CS molecules.[41] Additionally, compared with the CST/GO-0, COST/GO-0 has a new peak at the 1743 cm^{-1}, which attributed to the C=O stretching vibration. This indicated that the hydroxyl groups of C-6 positions of ST were oxidized and the carboxyl groups were introduced.[38,42]

As shown in Figure 1(b), in FTIR spectra of CST/GO-4 and COST/GO-4, the absorption peak of —OH stretching vibrations was at 3281, 3282 cm^{-1} respectively, which were higher than that of CST/GO-0

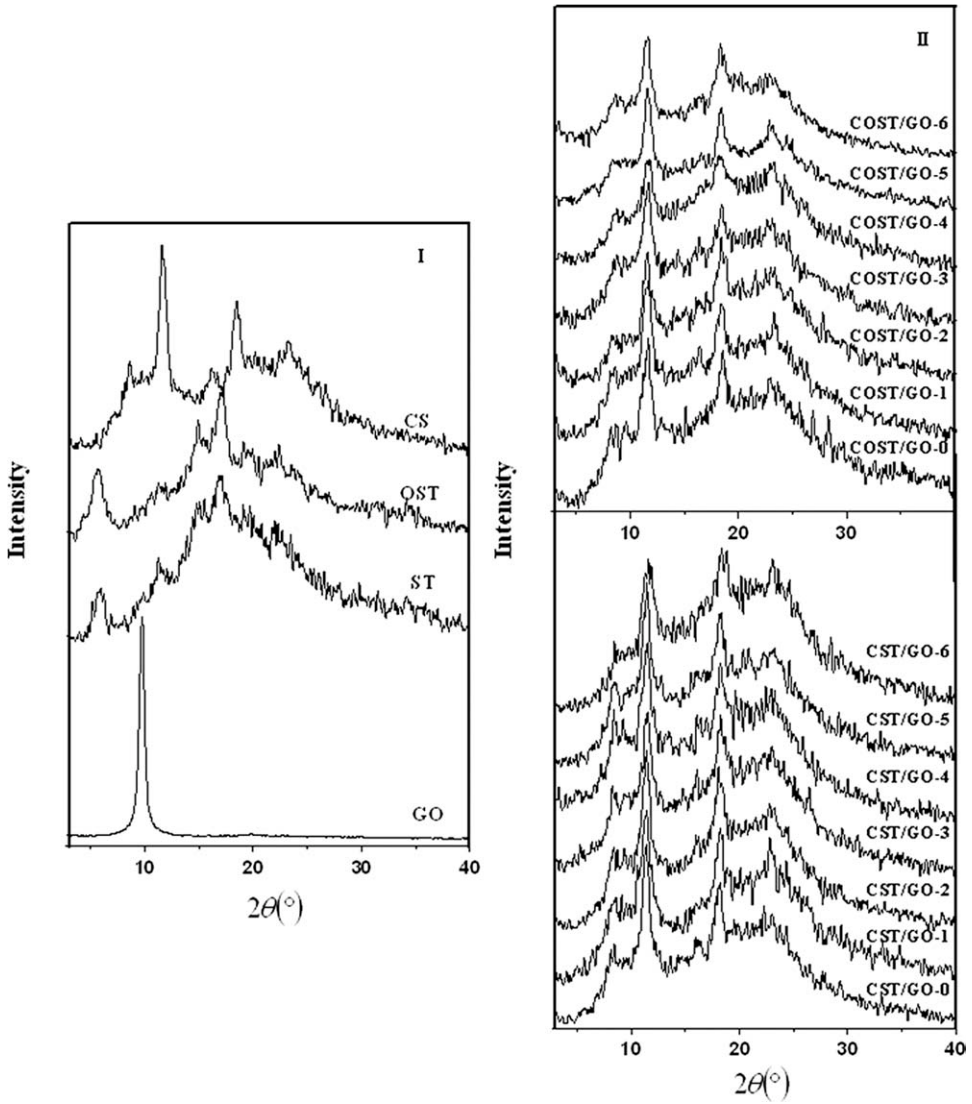

Figure 2 XRD patterns of original materials, COST/GO-*n*, and CST/GO-*n* nanocomposite films.

and COST/GO-0. Meanwhile, the δ_{OH} bending and CH_2 absorption bands shifted to higher wave numbers by small shifts compared to that of the CST/GO-0 and COST/GO-0. The similar phenomena have been discussed in other literature.[43,44] This important information indicated that the use of GO represents a physical cross-linking agent to obtain hydrogen bonded interacting polymers, which can promote the miscibility between OSR (ST) and CS molecules.

The XRD patterns of the original materials and resulting films are shown in Figure 2. In Figure 2(a), the characteristic XRD diffraction peak of GO sheets appeared at $2\theta = 11.5°$. The interlayer distance was estimated from Bragg's law, $2d \sin \theta = \lambda$, corresponding to a d-spacing of 0.77 nm.[45] For ST (only containing 30 wt % glycerol), the typical C-type crystalline pattern with peaks at $2\theta = 5.7°$ (characteristic of B type polymorphs), 15.1° (characteristic of A type polymorphs), 17.21° (characteristic of both A and B type polymorphs), 20.18° and 22.58° (characteristic of B type polymorphs) were observed clearly.[46,47]

Following the oxidation treatment, it can be observed that the crystallinity for OST was lower than that of ST (listed in Table I). It indicated that the strong intermolecular hydrogen bonding interactions between OST molecules effectively prevented the regular packing of the modified starch, and then the crystalline structure for starch was inflected by oxidation reaction. CS film shows two main diffraction peaks around $2\theta = 13.0°$ and 19.2° and two broad peaks around $2\theta = 9.2°$ and 25° with low intensity.[48]

Figure 2(b) shows the XRD patterns of CST/GO-*n* and COST/GO-*n* nanocomposites with various GO loadings. It is hard to find the characteristic peaks of GO in the composites, which indicated that GO was

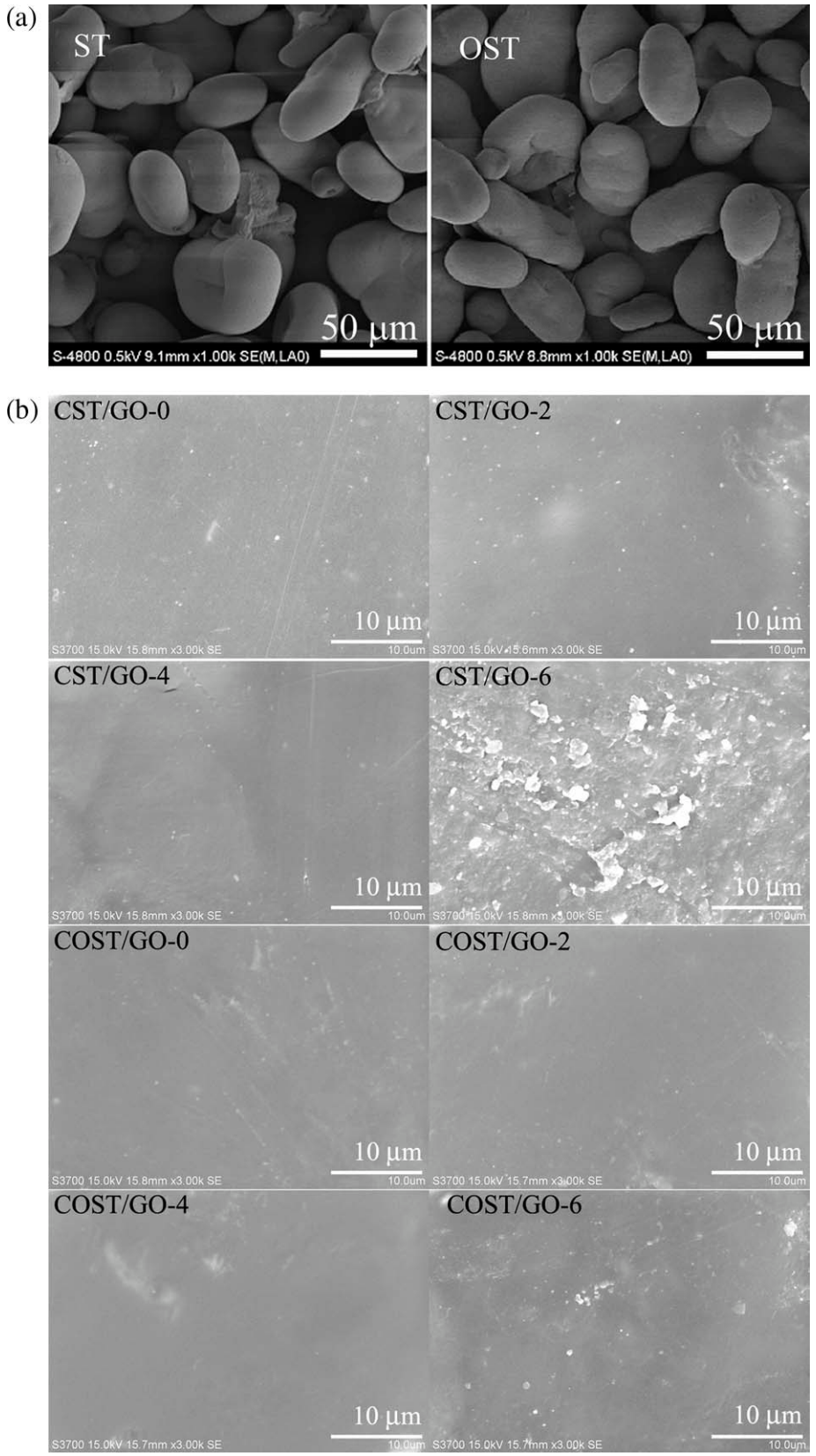

Figure 3 (a) SEM images for ST and OST powder. (b) SEM images of the surfaces of the films CST/GO-0, CST/GO-2, CST/GO-4, CST/GO-6, COST/GO-0, COST/GO-2, COST/GO-4, and COST/GO-6. (c) SEM images of fracture surfaces of the films CST/GO-0, CST/GO-2, CST/GO-4, CST/GO-6, COST/GO-0, COST/GO-2, COST/GO-4, and COST/GO-6.

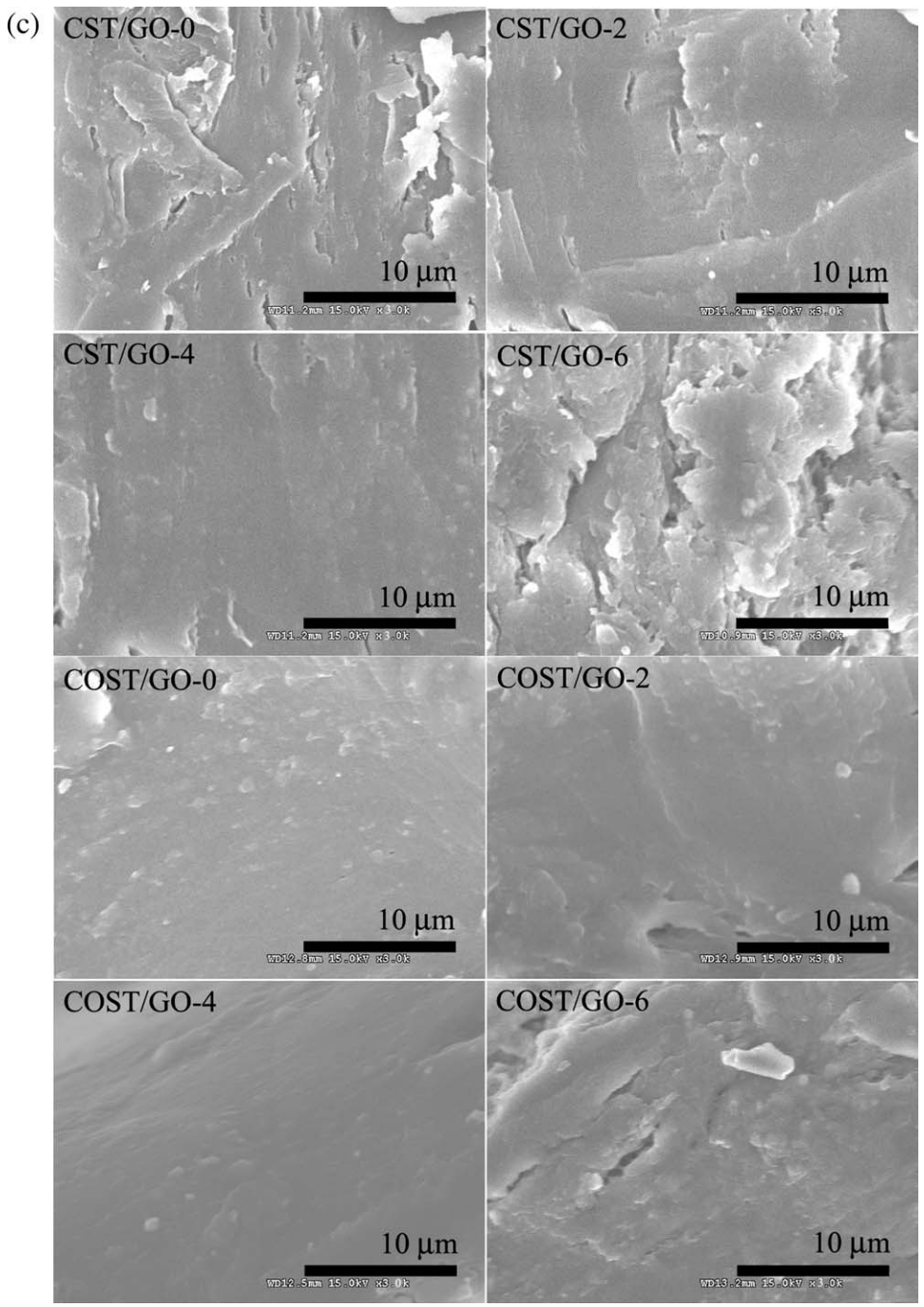

Figure 3 (Continued)

uniformly dispersed in blend matrix. For COST/GO-*n* composites, it can be observed that the diffraction pattern intensity was all slightly weaker compared with CST/GO-*n* composites. To reveal the effect of GO to the crystalline structure of OST-based and ST-based nanocomposites, the values of crystallinity for these nanocomposites were calculated and listed in Table I. From Table I, the values of crystallinity for OST-based composites were all lower than that of ST-based composites with the same loading of GO. It proved that GO nanosheets disturbed the parallel direction of the polymer chains because of strong hydrogen bonding interactions between them, and the best compatibility existed in the OST-based composite.

Morphological image analysis

SEM micrographs of ST powder and OST powder are shown in Figure 3(a). As shown in Figure 3(a), there was no obvious difference observed from the particle size and surface. Both of the starch and OST

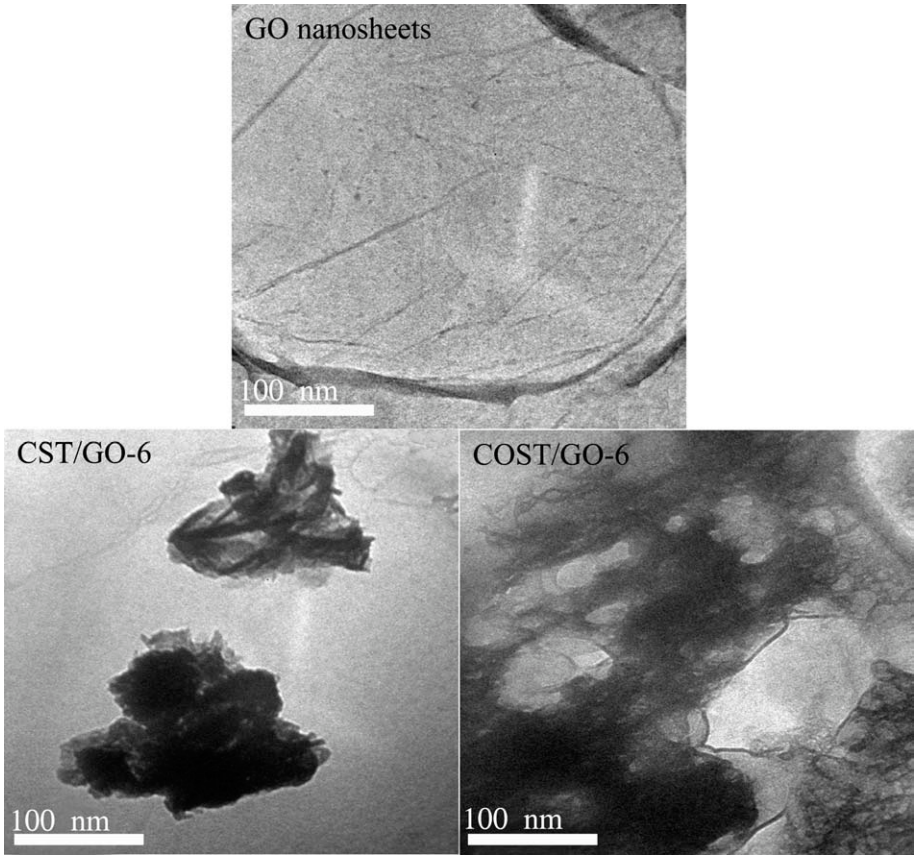

Figure 4 TEM micrographs of GO nanosheets, CST/GO-6, and COST/GO-6 nanocomposites.

particles were 20–40 μm in diameter and spherical or oval in shape according to literature.[49] The SEM photographs of the free surface of the selected films are shown in Figure 3(b). The selected films display a similar smooth surface. However, the CST/GO-6 and COST/GO-6 nanocomposite films exhibit rough surface and a certain degree of phase separation. This can be explained that higher loading of GO may result in aggregation of nanosheets, leading to the reduced compatibility between polymers. The fracture surface morphologies of the selected films are shown in Figure 3(c). It was observed that the cross-section of the CST/GO-0 film was very rough, indicating that ST and CS were not quite compatible, leading to phase separation of the two polymers. However, the fracture surface of the COST/GO-0 film was much smoother than that of CST/GO-0. Similar phenomena were also observed in CST/GO-2 and COST/GO-2 (CST/GO-4 and COST/GO-4), indicating that the compatibility of samples containing OST were significantly improved. Meanwhile, the cross-sections of CST/GO-4 and COST/GO-4 appear much smoother than the other nanocomposite films for the same series. This illustrated that GO formed a stronger interaction with the polymers and dispersed more homogenously in the matrix. However, it is found that the cross-sections of CST/GO-6 and COST/GO-6 were rough and phase separation appeared. This is due to the aggregation of GO nanosheets (discussed in Fig. 4). This could explain why the mechanical properties became worse when the GO loading was more than 2 wt %.

Figure 4 shows transmission electron microscopy (TEM) images of GO nanosheets, CST/GO-6 and COST/GO-6 composites. The central parts of the GO appear on TEM images as homogeneous and featureless region, whereas the edges of GO tend to scroll. In general, GO nanosheets tend to congregate together to form multilayer agglomerates.[50] For monolayer GO, a fold exhibits only one dark line. Scrolls and multiple folds can give rise to many number of dark lines even for monolayer GO, as indeed observed experimentally.[51] As shown in Figure 4, it is found that GO nanosheets in the size ranges of 150–200 nm aggregation in the CST/GO-6 and COST/GO-6 composite matrix. This can explain why both the tensile strength and Y_c reduced with higher GO loading (>2 wt %).

To observe the morphology of the surfaces of the films, the AFM micrographs of the CST/GO-0, CST/GO-4, COST/GO-0, and COST/GO-4 composites are shown in Figure 5. Surfaces of films were compared in terms of some of the roughness parameters, such as the mean roughness (R_a) and the root mean square of the Z data (R_q).[52] The mean roughness is

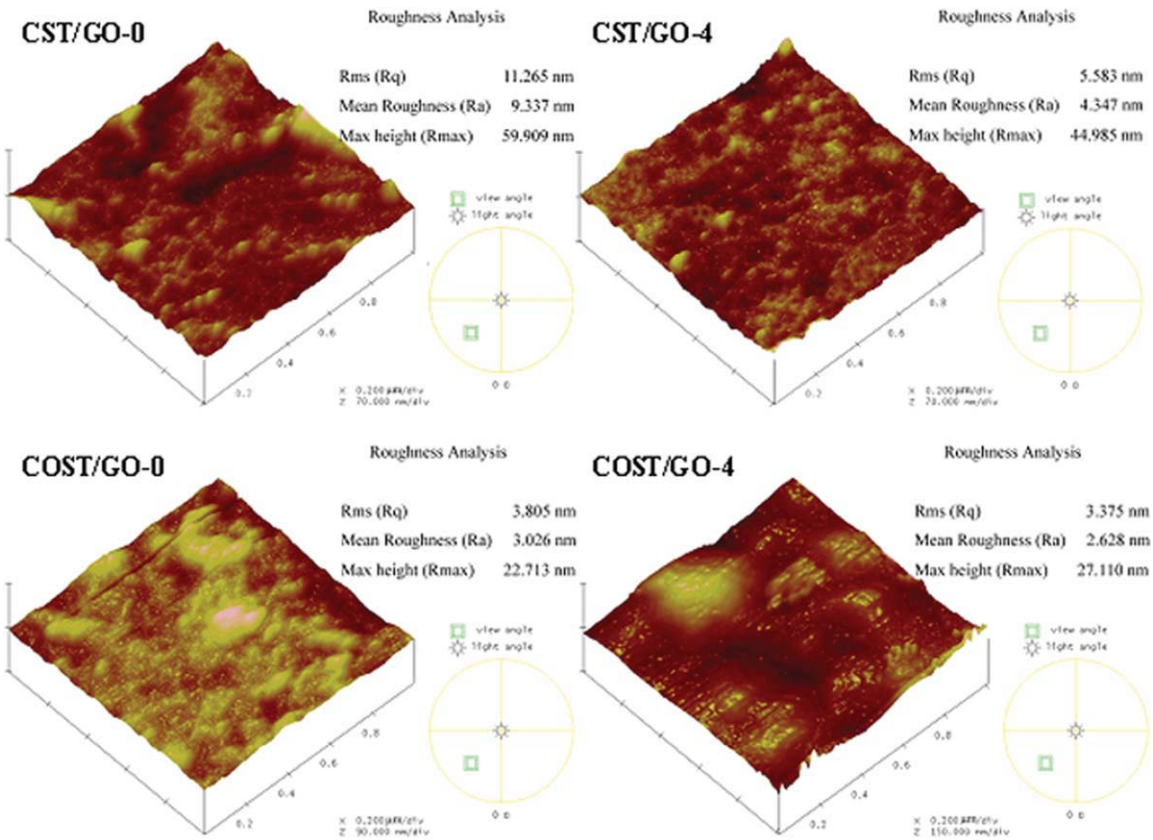

Figure 5 AFM images for the select films of COST/GO-*n* and CST/GO-*n*.[Color figure can be viewed in the online issue, which is available at wileyonlinelibrary.com.]

the mean value of surface relative to the center plane, the plane for which the volume enclosed by the image above and below this plane are equal, and is calculated as.[53]

$$R_a = \frac{1}{L_x L_y} \int_0^{L_y} \int_0^{L_y} |f(x,y)| \; dxdy \tag{2}$$

where f (x, y) is the surface relative to the center plane and L_x and L_y are the dimensions of the surface.

The root mean square of the Z values (R_q) is the standard deviation of the Z values within the given area and is calculated as

$$R_q = \sqrt{\frac{\sum (Z_i - Z_{\text{avg}})^2}{N}} \tag{3}$$

where Z_{avg} is the average of the Z values within the given area; Z_i, the current Z value; and N, the number of points within a given area. As shown in Figure 5, the surface morphologies of COST/GO-0 and COST/GO-4 composites were smoother and flatter, which were different from CST/GO-0 and CST/GO-4 film. The surface roughness parameters of COST/GO-0 and COST/GO-4 composites calculated by Nanoscope Multimode processing software, such as the mean roughness (R_a) and the root mean square of the Z data (R_q) were lower than that of CST/GO-0 (R_a = 9.337 nm, R_q = 11.265 nm) and CST/GO-4 (R_a = 4.347 nm; R_q = 5.583 nm), especially for the COST/GO-4 film with the lowest surface roughness parameters (R_a = 2.628 nm; R_q = 3.375 nm). The results indicated that the introduction of —COOH for starch favored the enhancement of the compatibility between OST and CS and the GO fillers. Moreover, the mean roughness (R_a) and the root mean square of the Z data (R_q) for CST/GO-4 and COST/GO-4 were also lower than that of CST/GO-0 and COST/GO-0 without GO fillers. This can be explained that the incorporation of GO also can improved the interaction between OST (starch) and CS molecules. This could be attributed to plenty of oxygen functional groups on the surface of GO, which were of benefit to form strong hydrogen bonding with both OST (ST) and CS molecules.

Thermal analysis

The thermal stability of the CST/GO-0 and COST/GO-*n* nanocomposites films was studied by TGA

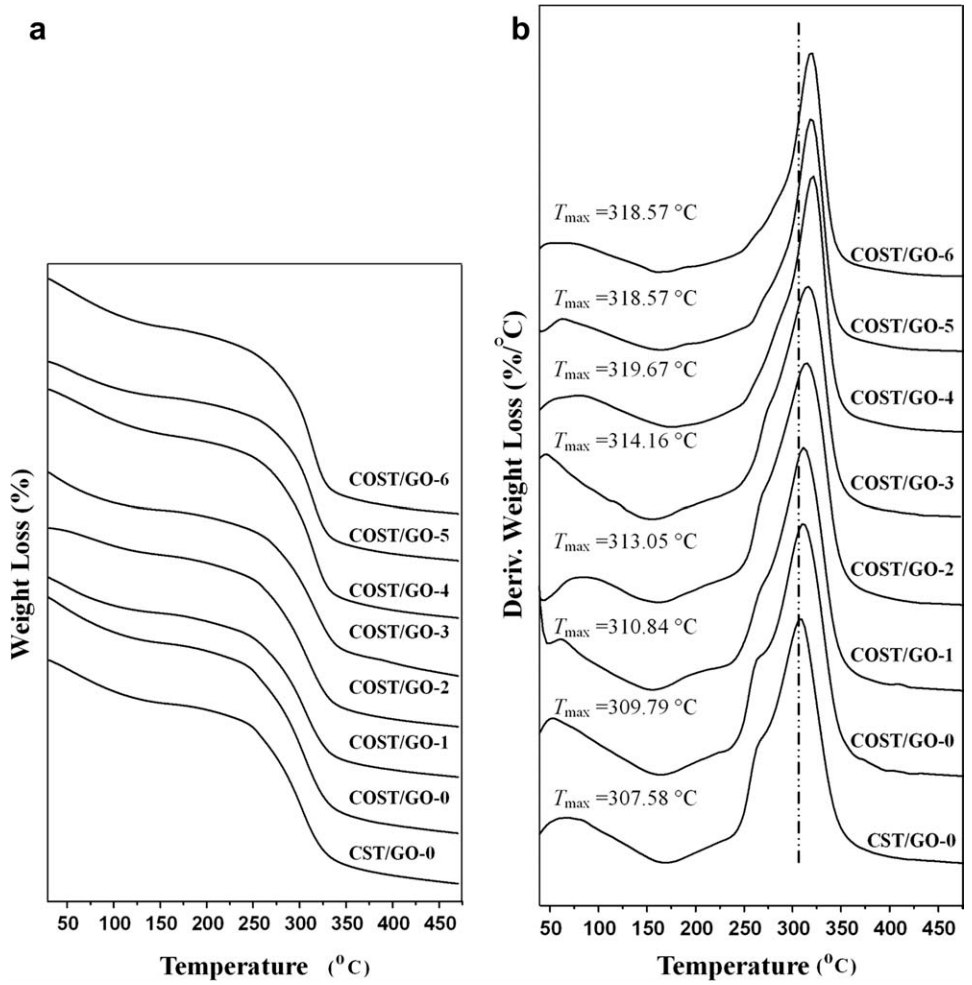

Figure 6 (a) TGA curves of CST/GO-0 and COST/GO-*n* nanocomposite films. (b) DTG curves of CST/GO-0 and COST/GO-*n* nanocomposite films.

and DTG shown in Figure 6(a,b), respectively. The initial weight loss of all samples, at 50–100°C, was due to evaporation of water and solvent, whereas the weight loss in the second range of 250–350°C corresponded to a complex process including the dehydration of the saccharide rings and depolymerization.[54–56] The temperatures of maximum loss ratio (T_{max}) for all samples are shown in Figure 6(b). Compared with CST/GO-0, the T_{max} shifted about 2°C higher for COST/GO-0 composite. It indicated that the introduction of —COOH for modified starch improved the interaction between CS and starch molecules leading to inhibit the motion of polymer chains. For COST/GO-*n* composites, when GO loading increased, the T_{max} of the blend films increased, as observed in Figure 6(b), indicating that the thermostability of the OST-based composites increased with increased GO loading in the films. When GO loading was higher than 2.0 wt %, the T_{max} of the blend films was slightly changed.

Mechanical properties

To illustrate the effect of carboxyl in OST on the mechanical properties of COST/GO-*n*, corresponding data of CST/GO-*n* were selected for control experimentation. Results for tensile strength, elongation at break and Young's modulus of the composites (CST/GO-*n* and COST/GO-*n* series) are presented in Figure 7(a–c). As GO loading increased, the tensile strength (σ_b) and Young's modulus (Y_c) for CST/GO-*n* composites increased, but the elongation at break (ε_b) of the biocomposites decreased. When GO loading varied from 0 to 2.0 wt %, the σ_b and Y_c increased from 11.40 MPa, 1.56 GPa to 16.29 MPa, and 7.30 GPa, respectively, while ε_b decreased from 88.18 to 32.96%. These results suggested that GO could improve the strength and stiffness of starch/CS-based composites at the expense of flexibility, which was similar to previous reports.[57,58] The improvement in the mechanical properties was due to the good dispersion of GO within the blend film and plenty of intermolecular hydrogen

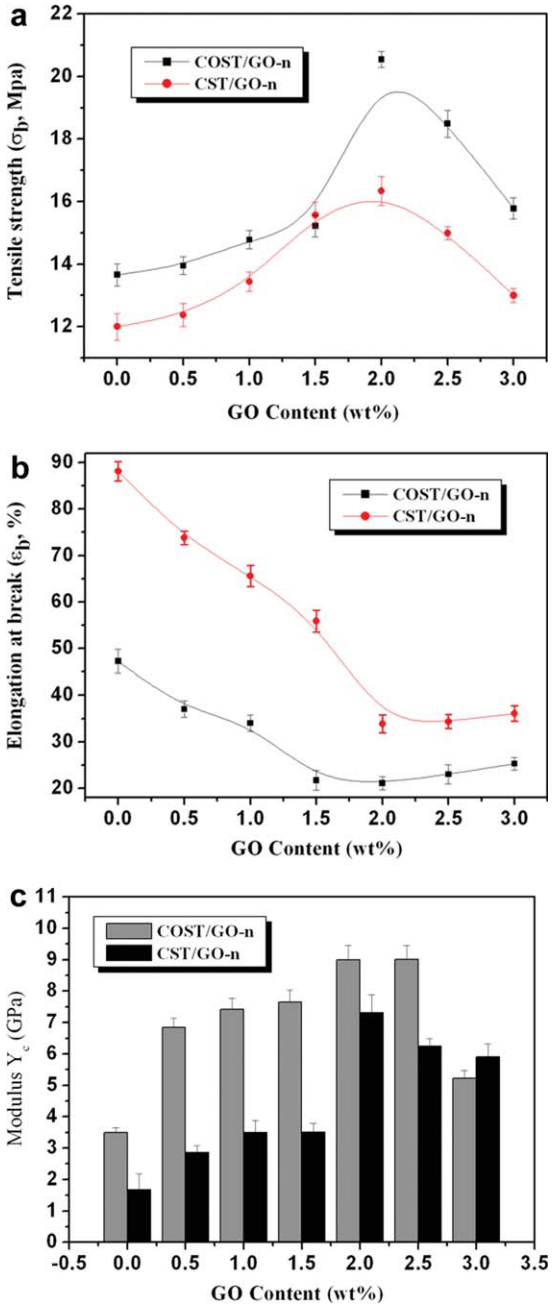

Figure 7 (a) Dependence of tensile strength of CST/GO-*n* and COST/GO-*n* nanocomposite films with different GO content. (b) Dependence of elongation at break of CST/GO-*n* and COST/GO-*n* nanocomposite films with different GO content. (c) Young's modulus (Yc) of CST/GO-*n* and COST/GO-*n* nanocomposite films as a function of mass fraction of GO. [Color figure can be viewed in the online issue, which is available at wileyonlinelibrary.com.]

bond sites formed between GO and ST/CS resulting in strong interactions among the components. Therefore, the miscibility was increased. So the mechanical properties of films were greatly improved. However, with greater GO loading (>2 wt %), both the tensile strength and Y_c reduced sharply, the reason for this might be the possible aggregation of nano-sized particles.

The COST/GO-*n* series blends had the same tendency as CST/GO-*n*. The σ_b and Y_c achieved a maximum of 21.54 MPa and 9.27 GPa when the GO loading was 2.0 wt %. Compared with the CST/GO-*n*, σ_b and Y_c were obviously higher, while ε_b was lower than that of CST/GO-*n* at the same loading of GO. It indicated that the carboxyl introduced by oxidation in the starch chain could improve the σ_b of COST/GO-*n* blends, but decreased the ε_b, which resulted from the strong hydrogen bonding among OST, CS, and GO. Strong intermolecular hydrogen bonding interactions formed between GO and OST/CS molecules and impact the recrystallize of the OST, thus the tensile strength was improved and the elongation at break was decreased.

Moisture uptake

The moisture uptake at equilibrium at 92% RH is plotted in Figure 8 for the blend films with and without oxidation. The influence of oxidation on the starch moisture absorption was clarified. It was observed that the MU value for CST/GO-0 and COST/GO-0 was 48.00 and 45.30%, respectively, indicating that OST and CS formed strong interactions through hydrogen bonding and electrostatic interaction, inhibiting permeation of water molecules into the blend film, and thus leading to the reduced MU. Moreover, when the GO was incorporated, moisture absorption of the both series became lower. This suggested that the addition of GO had an interactive effect with the base polymers and highly physical cross-linked structure with polymer molecules formed through the new hydrogen bonding, which diminished the number of available —OH groups for interaction with migrating water molecules. However, when the GO loading was greater 2.0–2.5 wt % loading, the moisture uptake increased with the increasing

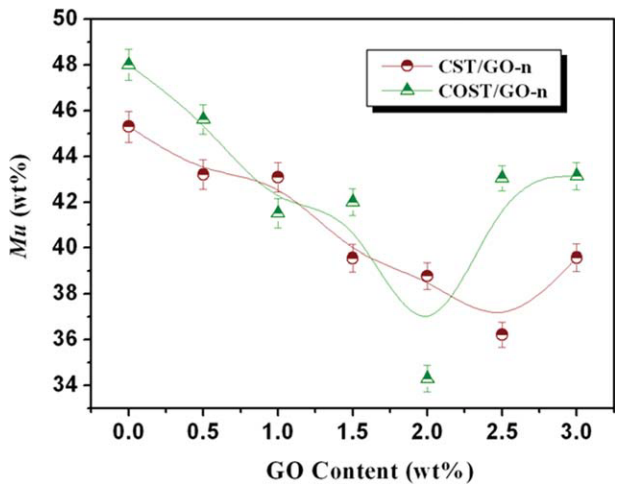

Figure 8 Moisture uptake at equilibrium of CST/GO-*n* and COST/GO-*n* nanocomposite films. [Color figure can be viewed in the online issue, which is available at wileyonlinelibrary.com.]

loading of GO, but not surpassing the COST/GO-0 (CST/GO-0) in the end. The reason for this might be that the aggregation of GO nanosheets and the content of hydrophilic —COOH groups increased moisture uptake with the increasing loading of GO. In a word, the results suggested that the appropriate loading of GO decreased the moisture uptake and improved water resistance of the nanocomposite films.

CONCLUSION

Two series of nanocomposite films (COST/GO-*n* and CST/GO-*n*) were prepared by a solution casting method. These results from FT-IR, XRD, AFM, and SEM indicated that the films of COST/GO-*n* showed better miscibility than CST/GO-*n*, which resulted in improved mechanical properties, thermal stability, and water-resistance. Tensile strength of the COST/GO-*n* nanocomposites increased from 13.66 to 21.54 MPa as the GO loading increased from 0 to 2.0 wt %. The presence of GO also decreased the MU and increased the degradation temperatures of the nanocomposites. Investigation suggested that the carboxyl groups introduced into the starch and the incorporation of GO can improve the properties of the starch-based composites due to the synergistic interaction and hydrogen bonding between GO, CS, and oxide starch.

References

1. Chang, P. R.; Jian, R. J.; Yu, J. G.; Ma, X. F. Carbohydr Polym 2010, 80, 420.
2. Sorrentino, A.; Gorrasi, G.; Vittoria, V. Trends Food Sci Technol 2007, 18, 84.
3. Chakraborty, S.; Sahoo, B.; Teraoko, I.; Miller, L. M.; Gross, R. A. Macromolecules 2005, 38, 61.
4. Guan, J.; Hanna, M. A. Ind Eng Chem Res 2005, 44, 3106.
5. Dust, J. M.; Gajda, A. M.; Flickinger, E. A.; Berkhalter, T. M.; Merchen N. R.; Fahey G. C. J Agr Food Chem 2004, 52, 2989.
6. Xu, Y. X.; Kim, K. M.; Hanna, M. A.; Nag D. Ind Crop Prod 2005, 21, 185.
7. Wu, Q. X.; Zhang, L. N. J Appl Polym Sci 2001, 79, 2006.
8. Spiridon, I.; Popescu, M. C.; Bodârlau, R.; Vasile, C. Polym Degrad Stab 2008, 93, 1884.
9. Martin, O.; Schwach, E.; Averous, L.; Courturier, Y. Starch--Starke 2001, 53, 372.
10. Shahidi, F.; Arachchi, J. K. V.; Jeon, Y. J. Trends Food Sci Technol 1999, 10, 37.
11. Shieh, Y. T.; Yang, Y. F. Eur Polym J 2006, 42, 3162.
12. Jia, Y. T.; Gong, J.; Gu, X. H.; Kim, H. Y.; Dong, J.; Shen, X. Y. Carbohydr Polym 2007, 67, 403.
13. Majeti, N. V.; Kumar, R. React Funct Polym 2000, 46, 1.
14. Wang, S. F.; Shen, L.; Tong, Y. J.; Chen, L.; Phang, I. Y.; Lim, P. Q. Polym Degrad Stab 2005, 90, 123.
15. Shen, X. L.; Wu, J. M.; Chen, Y. H.; Zhao, G. H. Food Hydrocolloids 2010, 24, 285.
16. Liu, F. J.; Qin, B.; He, L. G.; Song, R. Carbohydr Polym 2009, 78, 146.
17. Bourtoom, T.; Chinnan, M. S. LWT-Food Sci Technol 2008, 41, 1633.
18. Yoksan, R.; Chirachanchai, S. Mater Sci Eng C 2010, 30, 891.
19. Shaffer, M. S. P.; Windle, A. H. Adv Mater 1999, 11, 937.
20. Liu, T.; Phang, I. Y.; Shen, L.; Chow, S. Y.; Zhang, W. D. Macromolecules 2004, 37, 7214.
21. Park, J. H.; Jana, S. C. Polymer 2003, 44, 2091.
22. Yang, H.; Zhang, Q.; Guo, M.; Wang, C.; Du, R.; Fu, Q. Polymer 2006, 47, 2106.
23. Yu, A. P.; Ramesh, P.; Itkis, M. E.; Bekyarova, E.; Haddon, R. C. J Phys Chem C 2007, 111, 7565.
24. Liu, Q.; Liu, Z. F.; Zhang, X. Y.; Yang, L. Y. Adv Funct Mater 2009, 19, 894.
25. Raghu, A. V.; Lee, Y. R.; Jeong, H. M.; Shin, C. M. Macromol Chem Phys 2008, 209, 2487.
26. William, S.; Hummers, J. R.; Richard, E. J Am Chem Soc 1958, 80, 1339.
27. Hirata, M.; Gotou, T.; Ohba, M. Carbon 2005, 43, 503.
28. Szabo, T.; Berkesi, O.; Dekany, I. Carbon 2005, 43, 3186.
29. Lerf, A.; He, H.; Forster, M.; Klinowski, J. J Phys Chem B 1998, 102, 4477.
30. Lerf, A.; He, H.; Riedl, T.; Forster, M.; Klinowski, J. Solid State Ionics 1997, 101, 857.
31. Hontoria-Lucas, C.; Lopez-Peinado, A. J.; Lopez-Gonzalez, J. Dd.; Rojas-Cervantes, M. L.; Martin-Aranda, R. M. Carbon 1995, 33, 1585.
32. He, H.; Klinowski, J.; Forster, M.; Lerf, A. Chem Phys Lett 1998, 287, 53.
33. He, H.; Riedl, T.; Lerf, A.; Klinowski, J. J Phys Chem 1996, 100, 19954.
34. Bourlinos, A. B.; Gournis, D.; Petridis, D.; Szabó, T.; Szeri, A.; Dékány, I. Langmuir 2003, 19, 6050.
35. Stankovich, S.; Dikin, D. A.; Piner, R. D.; Kohlhass, K. M.; Kleinhammes, A. Carbon 2007, 45, 1558.
36. Nethravathi, C.; Rajamathi, J. T.; Ravishankar, N.; Shivakumara, C.; Rajamathi, M. Langmuir 2008, 24, 8240.
37. Szabo, T.; Szeri, A.; Dekany, I. Carbon 2005, 43, 87.
38. Huang, T. G.; Jiang, Q. M.; Zhang, B. L. Henan Chem Ind 2006, 11, 26.
39. Chattopadhyay, S.; Singhal, R. S.; Kulkarni, P. R. Carbohydr Polym 1997, 34, 203.
40. Wang, G. X.; Shen, X. P.; Wang, B.; Yao, J.; Park, J. Carbon 2009, 47, 1359.
41. Yang, Y. J.; Liu, C. H.; Chang, P. R.; Chen, Y.; Anderson, D. P.; Stumborg, M. J Appl Polym Sci 2010, 115, 1089.
42. Wu, H. X.; Liu, C. H.; Chen, J. G.; Chen, Y.; Anderson, D. P.; Chang, P. R. J Appl Polym Sci 2010, 118, 3082.
43. Wang, X. Y.; Du, Y. M.; Luo, J. W.; Lin, B. F.; Kennedy, J. F. Carbohydr Polym 2007, 69, 41.
44. Li, L. H.; Deng, J. C.; Deng, H. R.; Liu, Z. L.; Xin, L. Carbohydr Res 2010, 345, 994.
45. Xu, Y. X.; Hong, W. J.; Bai, H.; Li, C.; Shi, G. Q. Carbon 2009, 47, 3538.
46. Chen, Y.; Cao, X. D.; Chang, P. R.; Huneault, M. A. Carbohydr Polym 2008, 73, 8.
47. Wang, S. J.; Yu, J. L.; Gao, W. Y. Am J Biochem Biotech 2005, 1, 207.
48. El-Khodary, A.; Oraby, A. H.; Abdelnaby, M. M. J Magn Magn Mater 2008, 320, 1739.
49. Li, J. H.; Vasanthan, T. Food Res Int 2003, 36, 381.
50. Wang, G. X.; Wang, B.; Park, J.; Yang, J.; Shen, X. P.; Yao, J. Carbon 2009, 47, 68.
51. Meyer, J. C.; Geim, A. K.; Katsnelson, M. I.; Novoselov, K. S.; Booth, T. J.; Roth, S. Nature 2007, 446, 60.
52. Khulbe, K. C.; Kruczek, B.; Chowdhury, C.; Cacne, S.; Matsuura, T. J Appl Polym Sci 1996, 59, 1151.
53. Kesting, R. E. J Appl Polym Sci 1990, 41, 2739.
54. Mathew, A. P.; Dufresne, A. Biomacromolecules 2002, 3, 609.
55. Schlemmer, D.; Angélica, R. S.; Sales, M. J. A. Compos Struct 2010, 92, 2066.
56. Ma, X. F.; Chang, P. R.; Yu, J. G.; Stumborg, M. Carbohydr Polym 2009, 75, 1.
57. Yu, J. G.; Yang, J. W.; Liu, B. X.; Ma, X. F. Bioresour Technol 2009, 100, 2832.
58. Ma, X. F.; Yu, J. G.; Wang, N. Compos Sci Technol 2008, 68, 268.